Gap Opening of Graphene by Dual FeCl 3 -Acceptor and K-Donor Doping.

ARTICLE *in* JOURNAL OF PHYSICAL CHEMISTRY LETTERS · JANUARY 2011

Impact Factor: 7.46

4 AUTHORS, INCLUDING:

Geunsik Lee
Pohang University of Science and Technology
61 PUBLICATIONS **1,159** CITATIONS
SEE PROFILE

Jun Sung Kim
Pohang University of Science and Technology
76 PUBLICATIONS **914** CITATIONS
SEE PROFILE

Kwang-Sun Kim
Korea University of Technology and Education
555 PUBLICATIONS **30,634** CITATIONS
SEE PROFILE

THE JOURNAL OF PHYSICAL CHEMISTRY Letters

LETTER

pubs.acs.org/JPCL

Gap Opening of Graphene by Dual $FeCl_3$-Acceptor and K-Donor Doping

Jae Won Yang,[†] Geunsik Lee,[*,‡] Jai Sam Kim,[*,†] and Kwang S. Kim[*,†,‡]

[†]Department of Physics and [‡]Department of Chemistry, Pohang University of Science and Technology, Pohang 790-784, Republic of Korea

ABSTRACT: The band gap opening of graphene is the most desired property in the device industry because it is vital to the application of graphene as a logical device of semiconductors. Here, we show how to make a reasonably wide band gap in graphene. This is accomplished with bilayer graphene (BLG) dual-doped with $FeCl_3$-acceptor and K-donor. To elucidate this phenomenon, we employed the first-principles method taking into account van der Waals interaction. For the $FeCl_3$ adsorbed BLG, the optimal distance between the adjacent graphene and $FeCl_3$ layers is 4.6−4.8 Å, consistent with experiments. Due to the high electronegativity of $FeCl_3$, these graphene layers are hole-doped. The dual-doped BLG gives a band gap of 0.27 eV due to broken symmetry, with a Dirac point shift by −0.09 eV. This increased band gap and proper Dirac point shift could make the dual-doped BLG useful for applications toward future field effect transistor devices.

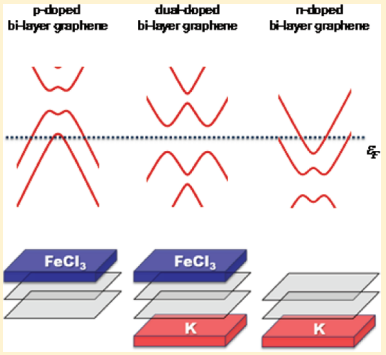

SECTION: Electron Transport, Optical and Electronic Devices, Hard Matter

Graphite intercalation compounds (GICs) are formed by a graphite host material and intercalants.[1] Their intriguing properties have attracted much interest due to various potential applications. For example, chemically inactive graphite layers could be used to maintain the pristine chemical and physical properties of intercalants. The weak binding between graphene and intercalant layers and the high interlayer surface area of graphite make GICs a good candidate for anode materials of the Li ion battery. Recently graphene was shown to exhibit interesting electron and spin transport phenomena, such as high carrier mobility, linear dispersion, pseudo spin chirality, and useful applications such as electronic/spin devices, touch panels, biosensors, solar cells, removal of hazardous materials, and fast DNA sequencing.[2−14] In realizing graphene-based transistors with its intriguing carrier transport property, one important issue is to obtain a finite energy gap.[15−23] The intercalation can be used to break the sublattice symmetry to open a gap. Furthermore, if we choose a transition metal compound as an intercalant, magnetically coupled transport could be observed if the exchange coupling between graphene and intercalating layers is strong enough.

Recently a transport measurement has been reported for bilayer graphene (BLG) with a magnetic intercalant of $FeCl_3$.[24] Despite a quite long history of more than 30 years for $FeCl_3$ intercalated graphite, little is known about its electronic or magnetic properties. This is partly due to ambiguous or even controversial atomic structures reported so far. An X-ray diffraction study reported a graphene interlayer distance of 9.37 Å,[25] when the number ratio of graphene and $FeCl_3$ layers is equal to 1, that is, stage 1. Each $FeCl_3$ layer behaves as an electron acceptor in the intercalated compound, thus the graphene layers will be hole-doped, where the doping amount would vary depending on the intercalation stage.[26,27] From a recent Hall measurement on the $FeCl_3$ intercalated BLG, the hole carrier density was as high as 5×10^{13} cm^{-1}.[24] Unfortunately, the graphene Dirac point was far beyond the back gate voltage accessible to this experiment. In order to examine the application as a field effect transistor (FET), it would be vital to studying the presence of band gap.

The increased electron density in the $FeCl_3$ intercalating layer causes additional complexity in the magnetic structure of the $FeCl_3$ intercalated graphite,[24,28−32] where noncollinear magnetic ordering transition at 15 K has been suggested in the case of a pristine $FeCl_3$ layered compound.[33] The doping dependency of the magnetic structure is related to the fact that the Fe spin moment will be changed by the electrons transferred to either Fe or Cl ions, where the respective key interaction is the Hund or superexchange coupling. Thus the doping amount is crucial information needed to study the electronic and magnetic structures. Importantly, it has been reported that for metal−graphene interfaces the amount of doping significantly depends on the distance between a graphene layer and a metal substrate, indicating the importance of chemical interaction even at a large distance greater than 3.0 Å.[34] Thus, an important step prior to the electronic structure study is to find the equilibrium distance relying on the first-principles method.

The experimental distance between layers is 5.81 Å for the bulk $FeCl_3$ and 4.69 Å for $FeCl_3$ intercalated graphite of the stage 1.[25,35,36] The known stacking sequence is the AB type with the graphene layers shifted laterally each other. The bulk $FeCl_3$ has the ABC stacking sequence with a = 6.06 Å and c = 17.42 Å with

Received: August 13, 2011
Accepted: September 23, 2011

Table 1. Interlayer Distances of the Three Reference Systems and the $FeCl_3$ Adsorbed BLG (aBLG) for Various Exchange-Correlation Functionals Which Are Compared with the Experimental Values (NA: not applicable)[a]

	PBE	revPBE	PBE+vdW-DF	revPBE+vdW-DF	average vdW-DF	experiment
bulk $FeCl_3$	6.48	7.67	5.54	5.83	5.69	5.81[36]
graphite	4.55	>6	3.39	3.55	3.47	3.35[1]
iMLG	5.35	5.67	4.61	4.79	4.70	4.69[25,35]
aBLG	5.27	5.71	4.62	4.80	4.71	NA

[a] Distances are in Å. The four approximations include normal GGA (PBE or revPBE) and its hybrid forms including the van der Waals interaction (PBE +vdW-DF or revPBE+vdW-DF). In the case of graphite with revPBE, the equilibrium point could not be found up to 6 Å.

weak van der Waals type layer−layer interaction. On the basis of density functional theory (DFT) calculations, such as local density approximation (LDA) or generalized gradient approximation (GGA), its calculated interlayer distance for the $FeCl_3$ GIC is 4.51 Å or 5.35 Å, respectively, where GGA predicts much longer binding distances. The partial agreement by the LDA method is due to the overestimated binding compensating the neglection of the van der Waals interaction, while a poor agreement by GGA is due to no compensation of the neglected van der Waals interaction. Thus, to obtain a good agreement with experiment, it is important to consider the van der Waals interaction correctly.

In this study, we use DFT plus van der Waals density functional (vdW-DF)[37−41] to calculate atomic structures of graphene and $FeCl_3$ layered composite systems with a proper treatment of the van der Waals interaction. After obtaining the optimized structures, we additionally provide GGA band structures with detailed analysis of charge transfer characters. Also, the gap opening will be studied for its probable application as FET devices. Our correct prediction of the gap size by including van der Waals interaction in DFT calculations is vital, because the gap depends significantly on the interlayer distance, as will be shown.

The interaction of graphene and $FeCl_3$ layers is calculated by using the periodic slab model. The lateral dimension of the hexagonal supercell is chosen to be 5×5 (2×2) of the graphene ($FeCl_3$) primitive cell. This makes the lattice mismatch as small as 1%, and the resulting stoichiometry C_6FeCl_3 is close to the experimental one, $C_{6.06}FeCl_3$ for GIC. A large vacuum region (>10 Å) is included along the vertical direction to eliminate unphysical interaction between periodic images of the layered composite.

We find the optimal interlayer distance by calculating total energies at various interlayer distances by taking into account the van der Waals interaction. A prior step is to relax the lateral atomic positions at a given interlayer distance. We use the Vienna ab initio simulation package (VASP)[42] to obtain the relaxed geometry, and additionally the associated electron density which will be used to calculate the van der Waals interaction energy. The projector augmented wave (PAW)[44] pseudopotential is used with the plane wave cutoff energy of 400 eV, and the exchange-correlation energy is approximated by the semilocal Perdew−Burke−Ernzerhof (PBE).[43,45] In the case that the layered composite does not have mirror symmetry along the vertical direction, the dipole correction is included. Only Γ-point sampling is used in the first Brillouin zone. After relaxation, we have seen that Cl atoms move to either hollow or bridge sites of graphene layers, which were initially at low symmetry positions determined from our unit cell construction.

The van der Waals energy is calculated with a postprocessing tool called the JuNoLo (Jülich Non Local) Code.[37−39] The vdW-DF total energy can be calculated as

$$E_{tot}^{vdW\text{-}DFT} = E_{tot}^{PBE} + \varepsilon^{revPBE}(-E_x^{PBE} + E_x^{revPBE}) + (-E_c^{PBE} + E_c^{LDA} + E_c^{NL}) \quad (1)$$

In eq 1, $E_x$and E_c denote the exchange and correlation energy respectively, where the van der Waals interaction (coupled dynamic fluctuations of electron density in separated regions) belongs to the correlation part. Starting from the PBE exchange-correlation, its correlation part (E_c^{PBE}) is subtracted, and the local and nonlocal correlation parts are added via E_c^{LDA} and E_c^{NL}, respectively, in the case of zero weight of revPBE functional ($\varepsilon^{revPBE} = 0$). In the case of full revPBE weight ($\varepsilon^{revPBE} = 1$), which is known as a good approximation for the exchange energy,[45] one has to subtract the original PBE exchange energy and add the revPBE exchange part. The nonlocal correlation term (E_c^{NL}) in eq 1, which includes the van der Waals interaction, is calculated by the following equation:

$$E_c^{NL} = \frac{1}{2}\int d^3r\, d^3r' n(r)\phi(r,r')n(r') \quad (2)$$

In the kernel function, ϕ ($\mathbf{r} - \mathbf{r}'$), which depends on $\mathbf{r} - \mathbf{r}'$, the interaction range has been carefully checked. We choose the range as large as 5 times the unit cell along the in-plane direction and 3 times that along the vertical direction, which gives a nonlocal correlation energy variation within 0.01 eV by increasing the range for bulk $FeCl_3$ and $FeCl_3$ GIC.

Our method is examined by computing the equilibrium interlayer distance for three reference systems such as graphite, bulk $FeCl_3$, and $FeCl_3$ intercalated graphite of stage I (iMLG: intercalated multilayer graphene). As our results are listed in Table 1, normal GGA methods (PBE or revPBE) predict larger distances than the available experimental value, where for bulk $FeCl_3$ the PBE predicts 11.7% larger than the experimental value and for graphite the revPBE could not find the energy minimum within the distance range up to 6 Å. However, the inclusion of van der Waals interaction gives much better agreement with the experiments. This indicates that the van der Waals interaction is a major element in stabilizing these systems. For the bulk $FeCl_3$, the vdW-DF with revPBE gives the least deviation from the experimental value, which is as small as 0.5%. For graphite, a better agreement has been obtained by PBE+vdW-DF rather than by revPBE+vdW-DF. In the case of the $FeCl_3$ intercalated graphite, the interlayer distance by PBE+vdW-DF or revPBE +vdW-DF is 4.61 Å or 4.79 Å with an average of 4.70 Å, which agrees well with the experimental value 4.69 Å, whereas normal DFT predicts much larger distances, either 5.35 or 5.67 Å.

Having confirmed the adequacy of our method, the equilibrium distance is computed for an artificial layered composite

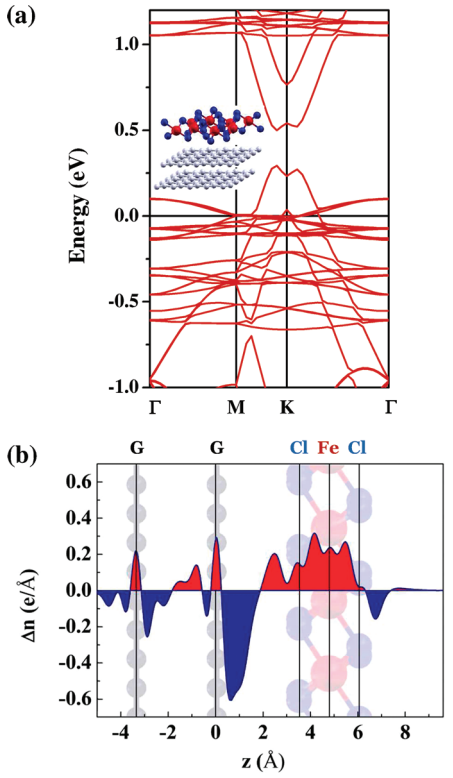

Figure 1. (a) Calculated band structures of aBLG exhibits a significant band gap opening. (b) The number of electrons for the composite system relative to those of separated reference systems. The transferred charge (in e/Å) along the c axis is summed over lateral positions inside the unit cell (5×5 or 2×2 layer unit cell for graphene or $FeCl_3$ layer). The vertical lines indicate the location of each layer for a given composite system. The graphene layers are at $z = 0.0$ Å, -3.35 Å, while the Fe atoms are at $z = 4.8$ Å with adjacent Cl atoms at $z = 3.45$ Å, 6.80 Å.

of the $FeCl_3$ adsorbed BLG (aBLG), shown in the inset of Figure 1a, which is expected to have a significant energy gap due to asymmetry. From our calculated total energies versus the distance between $FeCl_3$ and the nearby graphene layer by fixing the BLG distance, the equilibrium distance is predicted to be 4.71 Å. It is quite similar to that obtained for an iMLG system.

At the equilibrium distance for an aBLG, the electronic structure is calculated with the PBE exchange-correlation functional, which is shown in Figure 1a. It has a band gap of 0.21 eV near the K point. Its origin is the potential energy difference between two graphene layers (Δ = 0.31eV). The band gap is significantly affected by the interlayer distance. For example, it is 0.17 eV (-19%) if we use PBE optimize distance (5.27 Å), or 0.15 eV (-29%) for the revPBE case (5.71 Å). This indicates the significance of van der Waals interaction in the theoretical prediction of band structures.

In addition, we note upshift of graphene-related bands compared to the ideal graphene. This indicates significant hole doping, which is caused by the higher work function (6.22 V from our result) of the $FeCl_3$ layer than graphene (4.45 V). Thus, the details of charge transfer are analyzed by counting the number of electrons within each interval of real space grid along the c direction and subtracting the number of electrons of an isolated reference system where each layer resides at the same z position as in the composite system. As shown in Figure 1b, the increase of electrons can be seen mainly in Fe and Cl atomic sites

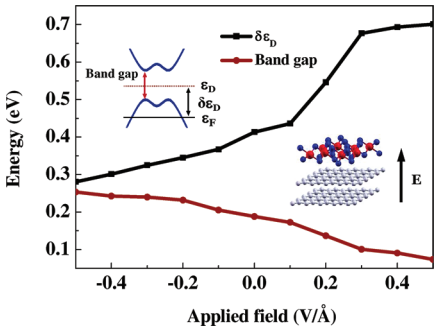

Figure 2. Variation of the Dirac point shift ($\delta\varepsilon_D$) and the band gap size as a function of applied external electric field along the c direction in the aBLG system (ε_F: Fermi energy). Inset: Schematic band structure of aBLG showing the band gap and the Dirac point shift.

as well as in bonding orbitals of Fe and Cl. Also poor screening of the first graphene layer induces substantial density variation at the second graphene layer.

By using the gap opening in aBLG, we may apply this system for FET devices. However, the Dirac point shift by 0.41 eV is beyond experimentally accessible doping range, where typical devices exhibit 0.3 eV shift at 100 V gate voltage. Also the gap size of 0.21 eV is marginally small. By applying an external electric field, one can enhance or suppress the potential energy difference between two graphene layers, so that the gap size and the Dirac point shift can be changed. Thus, we calculated them as a function of applied electric field, which is shown in Figure 2. For the negative electric field, the Dirac point shift is suppressed, and the gap size is enhanced. At the field less than -0.4 eV/ Å, the gap size is increased to 0.25 eV and the Dirac point shift is decreased to 0.28 eV. Although the desired change has been obtained, this amount may not be sufficient for typical back-gate controlled device applications.

In order to better control the gap size and the Dirac point shift, one can make use of dual-doping for BLG. By putting the elements of lower electron affinity than carbon at the opposite side of the BLG, the resulting electron doping will suppress the Dirac point shift originally appearing in the aBLG system. For example, Figure 3b shows the band structure for the aBLG+K system doped by one K atom per unit cell in addition to the $FeCl_3$ doping, whose band structure is also shown in Figure 3a. The K atom is located at the hollow site with a height of 2.7 Å in each hexagonal supercell of 5×5 graphene primitive cell.[46] As for the K-graphene bonding, the van der Waals interaction is insignificant, while the ionic bonding feature is noted.[47] As indicated by different colored dots in Figure 3a,b, the characteristics of graphene-related bands is maintained between two systems, and the main changes are the gap size and the Dirac point shift. While the gap size and the Dirac point shift for the $FeCl_3$ doping case are 0.21 and 0.41 eV, respectively, those for the aBLG+K system are 0.27 eV and -0.09 eV, respectively. The dual-doping gives much better results, in particular, in the Dirac point shift, than the applyied electric field, as expected.

The reason for such better performance is analyzed by the tight-binding method. The nearest-neighbor hopping parameters within one graphene layer and between two layers are given by $\gamma_0 = -3.16$ eV[48] and $\gamma_1 = -0.33$ eV (from our fitting to the DFT band of BLG). Also for the potential energy difference Δ between two layers, we use our DFT results. A finite Δ is a main factor of the band gap, which can be expressed as

dx.doi.org/10.1021/jz201098u |J. Phys. Chem. Lett. 2011, 2, 2577–2581

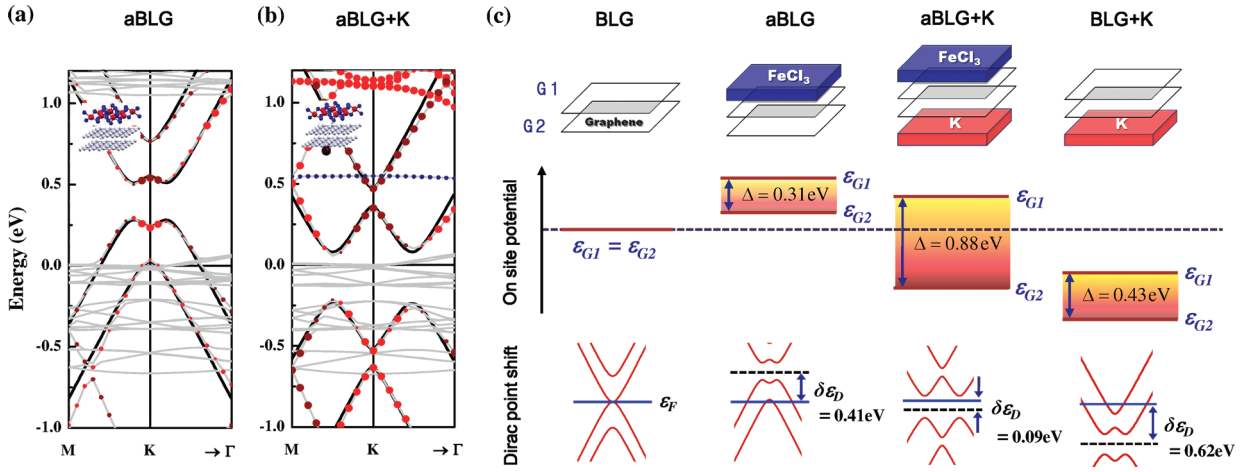

Figure 3. Calculated band structures of the BLG doped with $FeCl_3$ (aBGL) composite system (a) and the BLG dual-doped by $FeCl_3$ and K (aBLG+K) (b).[47] The gray line indicates the $FeCl_3$-major band, brown dots indicate the upper-graphene (G_1) band, and red dots indicate the lower-graphene (G_2) band. The band structure calculated by the tight binding method is plotted as a black line. The blue dots in panel b indicate the K-major band. Panel c represents the schematic models of the systems and the tight binding parameters for the onsite potential difference (Δ) and Dirac point shifts ($\delta\varepsilon_D$) obtained by DFT calculation.

$|\Delta|\gamma_1/(\Delta^2+\gamma_1^2)^{1/2}$, as in ref 15. From this formula, the band gaps are 0.23 and 0.32 eV by using Δ_{aBLG} = 0.31 eV and Δ_{aBLG+K} = 0.88 eV for the relevant systems shown in Figure 3a,b, respectively. These are consistent with the values from the DFT bands. In order to show good agreement between DFT and tight-binding methods, the tight-binding bands are represented by the solid line in Figure 3a,b. Here shifts are made in consideration of the incapability of doping effect by the tight binding method. This amount of shift can be regarded as the Dirac point shift, where they are 0.41 and −0.09 eV for Figure 3a,b, respectively. We notice that there is a slight difference in the gap size along two directions from K: one to Γ and the other to M. We attribute this directional dependence to the next-nearest hopping interactions between layers (γ_3). Figure 3c is a schematic summary of our results on doping induced gap.

Experimentally, such a gap opening due to different onsite potentials for BLG has been reported.[16,22] By covering K atoms onto BLG, a different number of electrons is doped at two layers, which induces the potential energy difference about 0.2 eV (band gap ∼0.2 eV).[16] Another one used a dual gate method to create the energy difference.[22] They showed a gap size of 0.25 eV attainable at the vertical field strength 3 V/nm. The gap size caused by the potential energy difference (Δ) will be maximized to γ_1 when Δ is much larger than γ_1. In the dual gate method, the maximally applicable voltage for a large Δ is limited due to the device safety. However, our dual molecular doping enables going beyond that limitation by properly choosing two compounds with a large work function difference. Also the parameter γ_1 may be increased by decreasing the interlayer distance in BLG with an additional intercalant of small atomic size. From these, one might satisfy the technological requirement for the gap size, 0.4 eV.[49]

In summary, by using the first principles method in consideration of the van der Waals interaction, we studied atomic and electronic structures of layered-composites of graphene and $FeCl_3$ and K. We find that the interlayer distance is 4.6−4.8 Å irrespective of the detailed structure of layers between graphene and $FeCl_3$. This indicates that the major contribution arises from the nearest interlayer interactions. From our calculated band structures, the graphene layers due to high electronegativity of intercalating $FeCl_3$ are hole-doped with a significant shift of the Dirac point. Also the asymmetric composite of BLG with the $FeCl_3$ layer adsorption is shown to exhibit an energy gap opening. Utilizing this asymmetric behavior, which increases the band gap, we find that the BLG with dual $FeCl_3$-acceptor and K-donor doping shows a larger energy gap opening (0.27 eV) with a proper Dirac point shift (−0.09 eV) toward practical FET device applications.

AUTHOR INFORMATION

Corresponding Author

*E-mail: kim@postech.ac.kr (K.S.K.); jsk@postech.ac.kr (J.S.K.); maxguen@postech.ac.kr (G.L.).

ACKNOWLEDGMENT

This work was supported by the NRF (National Honor Scientist Program: 2010-0020414, WCU: R32-2008-000-10180-0, Basic Science Research Program: 2011-0010186), Postech BSRI Research fund 2010, and KISTI (KSC-2011-G3-02).

REFERENCES

(1) Dresselhaus, M. S.; Dresselhaus, G. Intercalation Compounds of Graphite. *Adv. Phys.* **2002**, *51*, 1–186.

(2) Novoselov, K. S.; Geim, A. K.; Morozov, S. V.; Jiang, D.; Zhang, Y.; Dubonos, S. V.; Grigorieva, I. V.; Firsov, A. A. Electric Field Effect in Atomically Thin Carbon Films. *Science* **2004**, *306*, 666–669.

(3) Novoselov, K. S.; Geim, A. K.; Morozov, S. V.; Jiang, D.; Katsnelson, M. I.; Grigorieva, I. V.; Dubonos, S. V.; Firsov, A. A. Two-Dimensional Gas of Massless Dirac Fermions in Graphene. *Nature* **2005**, *438*, 197–200.

(4) Zhang, Y; Tan, Y; Stormer, H. L.; Kim, P. Experimental Observation of the Quantum Hall Effect and Berry's Phase in Graphene. *Nature* **2005**, *438*, 201–204.

(5) Kim, K. S.; Zhao, Y.; Jang, H.; Lee, S. Y.; Kim, J. M.; Kim, K. S.; Ahn, J.-H.; Kim, P.; Choi, J.-Y.; Hong, B. H. Large-Scale Pattern Growth of Graphene Films for Stretchable Transparent Electrodes. *Nature* **2009**, *457*, 706–710.

(6) Bae, S.; Kim, H.; Lee, Y.; Xu, X.; Park, J.-S.; Zheng, Y.; Balakrishnan, J.; Lei, T.; Ri Kim, H.; Song, Y. I.; et al. Roll-To-Roll

Production of 30-Inch Graphene Films for Transparent Electrodes. *Nat. Nanotechnol.* **2010**, *5*, 574–578.

(7) Park, J.; Lee, W. H.; Huh, S.; Sim, S. H.; Kim, S. B.; Cho, K.; Hong, B. H.; Kim, K. S. Work-Function Engineering of Graphene Electrodes by Self-Assembled Monolayers for High-Performance Organic Field-Effect Transistors. *J. Phys. Chem. Lett.* **2011**, *2*, 841–845.

(8) Cho, Y.; Choi, Y. C.; Kim, K. S. Graphene Spin-Valve Device Grown Epitaxially on the Ni(111) Substrate: A First Principles Study. *J. Phys. Chem. C* **2011**, *115*, 6019–6023.

(9) Sun, J. T.; Lu, Y. H.; Chen, W; Feng, Y. P.; Wee, A. T. S. Linear Tuning of Charge Carriers in Graphene by Organic Molecules and Charge-Transfer Complexes. *Phys. Rev. B* **2010**, *81*, 155403.

(10) Lu, Y. H.; Chen, W.; Feng, Y. P. Tuning the Electronic Structure of Graphene by an Organic Molecule. *J. Phys. Chem. B* **2009**, *113*, 2–5.

(11) Kim, W. Y.; Kim, K. S. Prediction of Very Large Values of Magnetoresistance in a Graphene Nanoribbon Device. *Nat. Nanotechnol.* **2008**, *3*, 408–412.

(12) Min, S. K.; Kim, W. Y.; Cho, Y.; Kim, K. S. Fast DNA Sequencing with a Graphene-Based Nanochannel Device. *Nat. Nanotechnol.* **2011**, *6*, 162–165.

(13) Cho, Y.; Min, S. K.; Kim, W. Y.; Kim, K. S. The Origin of Dips for the Graphene-Based DNA Sequencing Device. *Phys. Chem. Chem. Phys.* **2011**, *13*, 14293–14296.

(14) Lee, G.; Kim, K. S.; Cho, K. Theoretical Study of the Electron Transport in Graphene with Vacancy and Residual Oxygen Defects after High-Temperature Reduction. *J. Phys. Chem. C* **2011**, *115*, 9719–9725.

(15) McCann, E. Asymmetry Gap in the Electronic Band Structure of Bilayer Graphene. *Phys. Rev. B* **2006**, *74*, 161403.

(16) Ohta, T.; Bostwick, A.; Seyller, T.; Horn, K.; Rotenberg, E. Controlling the Electronic Structure of Bilayer Graphene. *Science* **2006**, *313*, 951–954.

(17) Castro, E.; Novoselov, K.; Morozov, S.; Peres, N.; dos Santos, J.; Nilsson, J.; Guinea, F.; Geim, A.; Neto, A. Biased Bilayer Graphene: Semiconductor with a Gap Tunable by the Electric Field Effect. *Phys. Rev. Lett.* **2007**, *99*, 216802.

(18) Han, M.; Özyilmaz, B.; Zhang, Y.; Kim, P. Energy Band-Gap Engineering of Graphene Nanoribbons. *Phys. Rev. Lett.* **2007**, *98*, 206805.

(19) Oostinga, J. B.; Heersche, H. B.; Liu, X.; Morpurgo, A. F.; Vandersypen, L. M. K. Gate-Induced Insulating State in Bilayer Graphene Devices. *Nat. Mater.* **2007**, *7*, 151–157.

(20) Wu, Y. Q.; Ye, P. D.; Capano, M. A.; Xuan, Y.; Sui, Y.; Qi, M.; Cooper, J. A.; Shen, T.; Pandey, D.; Prakash, G.; et al. Top-Gated Graphene Field-Effect-Transistors Formed by Decomposition of SiC. *Appl. Phys. Lett.* **2008**, *92*, 092102.

(21) Shemella, P.; Nayak, S. K. Electronic Structure and Band-Gap Modulation of Graphene via Substrate Surface Chemistry. *Appl. Phys. Lett.* **2009**, *94*, 032101.

(22) Zhang, Y.; Tang, T.-T.; Girit, C.; Hao, Z.; Martin, M. C.; Zettl, A.; Crommie, M. F.; Shen, Y. R.; Wang, F. Direct Observation of a Widely Tunable Bandgap in Bilayer Graphene. *Nature* **2009**, *459*, 820–823.

(23) Xia, F.; Farmer, D. B.; Lin, Y.-m.; Avouris, P. Graphene Field-Effect Transistors with High On/Off Current Ratio and Large Transport Band Gap at Room Temperature. *Nano Lett.* **2010**, *10*, 715–718.

(24) Kim, N.; Kim, K. S.; Jung, N.; Brus, L.; Kim, P. Synthesis and Electrical Characterization of Magnetic Bilayer Graphene Intercalate. *Nano Lett.* **2011**, *11*, 860–865.

(25) Thomas, J. M.; Millward, G. R.; Davies, N. C.; Evans, E. L. On "Seeing" the Stacking Sequence in Graphite-Iron(III) Chloride Intercalates by High-Resolution Electron Microscopy. *J. Chem. Soc.* **1976**, *23*, 2443–2445.

(26) Pietronero, L.; Strässler, S.; Zeller, H. R. Charge Distribution in *c* Direction in Lamellar Graphite Acceptor Intercalation Compounds. *Phys. Rev. Lett.* **1978**, *41*, 763–767.

(27) Safran, S. A.; Hamann, D. R. Electrostatic Interactions and Staging in Graphite Intercalation Compounds. *Phys. Rev. B* **1980**, *22*, 606–612.

(28) Ohhashi, K.; Tsujikawa, I. Magnetic Properties of $FeCl_3$—Graphite Compounds. I. Mössbauer Studies. *J. Phys. Soc. Jpn.* **1974**, *36*, 422–430.

(29) Simon, C.; Batallan, F.; Rosenman, I.; Schweitzer, J.; Lauter, H.; Vangelisti, R. Magnetic Order in $FeCl_3$ Intercalated Graphite by Neutron Diffraction. *J. Phys. Lett. (Paris)* **1983**, *44*, 641–647.

(30) Prietsch, M.; Wortmann, G.; Kaindl, G.; Schlögl, R. Mössbauer Study of Stage-2 $FeCl_3$—Graphite. *Phys. Rev. B* **1986**, *33*, 7451–7461.

(31) Suzuki, M.; Suzuki, I. S. Spin-Glass Phases in Stage-2 $FeCl_3$ Graphite Intercalation Compound. *Phys. Rev. B* **1998**, *58*, 371–384.

(32) Zhan, D.; Sun, L.; Ni, Z. H.; Liu, L.; Fan, X. F.; Wang, Y.; Yu, T.; Lam, Y. M.; Huang, W.; Shen, Z. X. $FeCl_3$-Based Few-Layer Graphene Intercalation Compounds: Single Linear Dispersion Electronic Band Structure and Strong Charge Transfer Doping. *Adv. Funct. Mater.* **2010**, *20*, 3504–3509.

(33) Kocher, C. W. Mössbauer Effect Study of Antiferromagnetic $FeCl_3$. *Phys. Lett. A* **1967**, *24*, 93–94.

(34) Giovannetti, G; K. Khomyakov, P. A.; Brocks, G.; Karpan, V. M.; van den Brink, J.; Kelly, P. J. Doping Graphene with Metal Contacts. *Phys. Rev. Lett.* **2008**, *101*, 026803.

(35) Ikemiya, N.; Okazaki, Y.; Hara, S. Cleaved Surface Structure of $CuCl_2^-$ and $FeCl_3^-$ Graphite Intercalation Compounds Detected by Atomic Force Microscopy. *Carbon* **1994**, *32*, 1191–1196.

(36) Hashimoto, S.; Forster, K.; Moss, S. C. Structure Refinement of an $FeCl_3$ Crystal Using a Thin Plate Sample. *J. Appl. Crystallogr.* **1989**, *22*, 173–180.

(37) Rydberg, H.; Dion, M.; Jacobson, N.; Schröder, E.; Hyldgaard, P.; Simak, S.; Langreth, D.; Lundqvist, B. van der Waals Density Functional for Layered Structures. *Phys. Rev. Lett.* **2003**, *91*, 126402.

(38) Dion, M.; Rydberg, H.; Schröder, E.; Langreth, D. C.; Lundqvist, B. I. van der Waals Density Functional for General Geometries. *Phys. Rev. Lett.* **2004**, *92*, 246401.

(39) Langreth, D. C.; Dion, M.; Rydberg, H.; Schröder, E.; Hyldgaard, P.; Lundqvist, B. I. van der Waals Density Functional Theory with Applications. *Int. J. Quantum Chem.* **2005**, *101*, 599–610.

(40) Thonhauser, T.; Cooper, V. R.; Li, S.; Puzder, A.; Hyldgaard, P.; Langreth, D. C. van der Waals Density Functional: Self-Consistent Potential and the Nature of the van der Waals Bond. *Phys. Rev. B* **2007**, *76*, 125112.

(41) Silvestrelli, P. L. van der Waals Interactions in DFT Made Easy by Wannier Functions. *Phys. Rev. Lett.* **2008**, *100*, 053002.

(42) Kresse, G.; Furthmüller, J. Efficient Iterative Schemes for Ab Initio Total-Energy Calculations Using a Plane-Wave Basis Set. *Phys. Rev. B* **1996**, *54*, 11169–11186.

(43) Perdew, J. P.; Burke, K.; Ernzerhof, M. Generalized Gradient Approximation Made Simple. *Phys. Rev. Lett.* **1996**, *77*, 3865–3868.

(44) Kresse, G.; Joubert, D. From Ultrasoft Pseudopotentials to the Projector Augmented-Wave Method. *Phys. Rev. B* **1999**, *59*, 1758–1775.

(45) Zhang, Y.; Yang, W. Comment on "Generalized Gradient Approximation Made Simple". *Phys. Rev. Lett.* **1998**, *80*, 890.

(46) Chan, K. T.; Neaton, J. B.; Cohen, M. L. First-Principles Study of Metal Adatom Adsorption on Graphene. *Phys. Rev. B* **2008**, *77*, 235430.

(47) Ziambaras, E.; Kleis, J.; Schröder, E; Hyldgaard, P. Potassium Intercalation in Graphite: A van der Waals Density-Functional Study. *Phys. Rev. B* **2007**, *76*, 155425.

(48) Toy, W. W.; Dresselhaus, M. S.; Dresselhaus, G. Minority Carriers in Graphite and the H-Point Magnetoreflection Spectra. *Phys. Rev. B* **1977**, *15*, 4077.

(49) Frank, S. Graphene Transistors. *Nat. Nanotechnol.* **2010**, *5*, 487–496.